Effect of Cu doping on the microstructure and mechanical properties of AlTiVN-Cu nanocomposite coatings

MEI, Haijuan, GENG, Dongsen, WANG, Rui, CHENG, Lixia, DING, Ji Cheng, LUO, Quanshun <http://orcid.org/0000-0003-4102-2129>, ZHANG, Teng Fei <http://orcid.org/0000-0003-3819-4042> and WANG, Qimin

Effect of Cu doping on the microstructure and mechanical properties of AlTiVN-Cu nanocomposite coatings

Haijuan Mei [a,b], Dongsen Geng [a], Rui Wang [a], Lixia Cheng [b],

Ji Cheng Ding [c], Quanshun Luo [d], Teng Fei Zhang [a], Qimin Wang [a,*]

[a] *School of Electromechanical Engineering, Guangdong University of Technology, Guangzhou, China*

[b] *Guangdong Provincial Key Laboratory of Electronic Functional Materials and Devices, Huizhou University, Huizhou, China*

[c] *School of Convergence Science, Pusan National University, Busan 609-735, South Korea*

[d] *Materials and Engineering Research Institute, Sheffield Hallam University, Sheffield, S1 1WB, UK*

* Corresponding author: qmwang@gdut.edu.cn (Qimin Wang).

ABSTRACT

Cu phase has been incorporated into hard coatings to form nanocomposite structure, which not only enhanced the hardness but also the toughness due to excellent ductility of copper. In this study, a single $Al_{67}Ti_{33}$-V-Cu spliced target was used to prepare the AlTiVN-Cu nanocomposite coatings, and the effect of Cu doping on microstructure and mechanical properties of AlTiVN-Cu coatings has been investigated. The results showed that the deposition rate linearly increased from 3.8 to 13.4 nm/min when Cu content increased from 2.6 to 46.7 at.%. AlTiVN-Cu coatings exhibited a Ti-Al-V-N solid-solution phase with strong (111) preferred orientation at low Cu contents below 8.3 at.%. When Cu content increased above 22.6 at.%, Cu atoms grew up into metallic crystallites and strongly suppressed crystal growth of nitride coatings due to repeated nucleation. With increasing Cu content, the microstructure transferred from compact columnar to dense featureless, and then to coarse columnar structure. AlTiVN-Cu(2.6 at.%) coating exhibited a super hardness of 41.1 GPa and an excellent toughness with a high H^3/E^{*2} ratio of 0.24.

Keywords: AlTiVN-Cu; Microstructure; Mechanical properties; Toughness.

1. Introduction

In last decades, ternary TiAlN coatings have been widely applied in cutting tools attribute to the high hardness, excellent wear resistance, good oxidation resistance and corrosion resistance at elevated temperatures [1–4]. To meet the increasing demand of modern machining technology under extreme conditions, especially for high-speed and dry cutting, some novel structures based on ternary TiAlN hard coatings, such as multicomponent alloying structure [5, 6], nanocomposite structure [7, 8], multilayer or nano-structure [9, 10], have been put forward to further improve the mechanical properties and wear resistant of the coatings.

To further enhance the oxidation resistant and thermal properties, some metallic elements with high melting point (e.g. Y, Ta, Hf) have been incorporated into TiAlN hard coatings, which was related to promoting the formation of Al_2O_3 dense layer [11, 12]. Lubricious oxides with substoichiometric compounds were commonly referred to as Magnéli phases (e.g. Mo, W, V) [13]. Due to the rapid oxidation of VN coatings at elevated temperatures above 500 °C [14], the formation of vanadium oxides including V_2O_5 and Magnéli phases from the series V_nO_{2n-1} was

beneficial for providing lubricious effects, and V was incorporated into TiAlN hard coatings to improve the tribological properties [15]. However, the V-addition promoted the formation of rutile-like TiO_2 instead of a dense Al_2O_3, resulting in a drop in oxidation resistance [6, 16]. In addition, the alloying of V was found to further increase the coating hardness due to solid solution hardening of fcc Ti-Al-V-N phase [17]. Moreover, increasing V content reduced the fraction of hcp AlN phases in the dual-phase (fcc/hcp) structure, causing a significant hardness enhancement from 21 to 27.5 GPa for $Ti_{33-x}Al_{67}V_xN$ coatings [18]. Although the hardness of TiAlN coatings have been improved by the V addition, but suffered from an increased flank wear due to the increase of brittleness for Ti-Al-V-N coatings [19]. Similar results were also found in the Ti-V-N coatings that a high V content led to a decrease in ductility of the coatings [20].

Recently, some soft phases (e.g. Cu, Ag, Ni) have been incorporated into hard coatings to form the nanocomposite structure, which simultaneously exhibited both high hardness and toughness [21]. Among which, it is well know that soft Cu phase exhibit excellent ductility, which could improve coating hardness and toughness [22, 23], or even lower the friction coefficient [24, 25]. It was reported by Jirout et al. [26] that the addition of Cu into ZrO_2 coatings altered the microstructure and macrostress, which significantly influenced mechanical properties, such as toughness or brittleness. Due to the grain boundaries in crystalline coatings promoted the propagation of cracks, amorphous Zr-Cu-O coating with high Cu content of 38 at.% exhibited better fracture toughness as compared to the polycrystalline coatings. In addition, the additive Cu as a soft and ductile metal has been reported to improve the coating hardness and tribological properties of (Ti,Al)N-Cu coatings [27]. Thus, it can be inferred that the comprehensive properties of Ti-Al-V-N multicomponent coatings could be improved by the addition of Cu to form a nanocomposite structure.

The aim of this work was to prepare AlTiVN-Cu coatings by high power impulse magnetron sputtering (HIPIMS) with a single $Al_{67}Ti_{33}$-V-Cu spliced target. A variation in Cu contents could be achieved simply by altering the vertical substrate positions, in order to study the effect of Cu doping on the deposition rate, microstructure, residual stress and mechanical properties of AlTiVN-Cu nanocomposite coatings.

2. Experimental

2.1. Coating deposition

AlTiVN-Cu coatings were deposited on 316L stainless steels and YT14 cemented carbides by high power impulse magnetron sputtering (HIPIMS) with a rectangular spliced target (69 mm × 443 mm), which was consisted of two metal targets of Cu and V (99.9% purity), and a $Al_{67}Ti_{33}$ alloy target (99.9% purity). As shown in Fig. 1, four different vertical substrate distances (D = 4, 10, 16, 22 cm) were designed to prepare AlTiVN-Cu coatings with various compositions, especially for the addition of V and Cu, similar to our previous studies for the design of Mo-V-Cu-N coatings [28]. Before deposition, all the samples were treated ultrasonically in anhydrous ethanol and then fixed on the different vertical position holders in the chamber after dried in air. The deposition process started with ion etching by Ar glow discharge at a DC bias voltage of −1000 V for 15 min. Then followed by the plasma bombardment with Cr^+, which was conducted by arc ion plating (AIP) with a Cr target (99.9% purity, Ø 100 mm) at a target current of 100 A for 3 min. To further enhance the adhesion strength, a thin inter-layer of CrN (~100 nm in thickness) was first deposited by AIP technique. Then AlTiVN-Cu coatings were deposited by HIPIMS technique in a common Ar and N_2 atmosphere. The deposition time was set as 180 min, and detail deposition parameter were listed in Table 1. The total coating thickness was in the range of 0.8 to 2.5 μm.

2.2. Coating characterization

A field emission scanning electron microscopy (FE-SEM, Quanta650) was used to characterize the coating surfaces and cross-sections, the coating compositions were measured by energy-dispersive X-ray spectrum (EDX). The deposition rates were calculated according to the

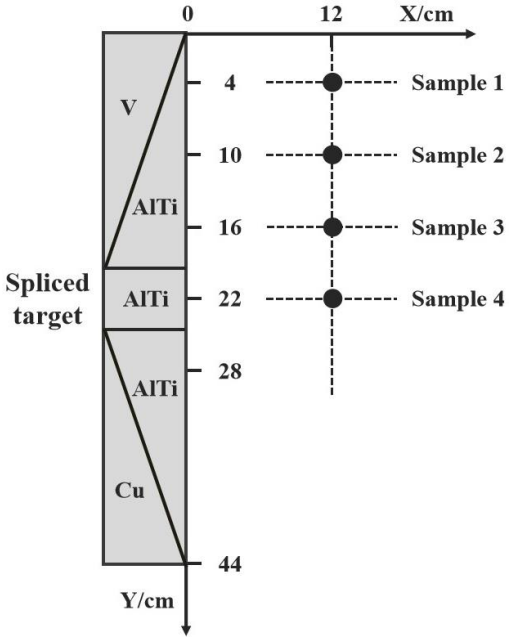

Fig. 1. Schematic diagram of $Al_{67}Ti_{33}$-V-Cu spliced target and the substrate positions.

Table 1 Deposition parameters of AlTiVN-Cu coatings deposited by HIPIMS.

Parameters	Values
Base pressure (Pa)	5.0×10^{-3}
Working pressure (Pa)	0.6
N_2 /Ar flow rate (sccm)	10 / 45
Working temperature (°C)	200
Bias voltage (V)	–100
Target power (kW)	1.5
Pulse length (μs)	100
Frequency (Hz)	200
Duty cycle	2%
Vertical substrate distance D (cm)	4、10、16、22
Deposition time (min)	180

coating thickness observed from the cross-sections. The crystal structure was measured by X-ray diffraction (XRD, D8 Advance) using Bragg Brentano mode and Cu K_a radiation. The instrument operated at 40 kV and 40 mA, and the scanning diffraction range was 20°–80° with a step size of 0.02°. An atomic force microscopy (AFM, Bruker) was used to measure the average surface roughness of the coatings, which were performed on a scan area of 5 × 5 μm^2 in a contact mode. The selected sample was further characterized by field-emission transmission electron microscopy (FE-TEM, Philips CM20) with tungsten electron gun operated at 200 kV. The cross-sectional sample was prepared by using a precision ion polishing system (model 691) with a low angle Ar^+ ion beam between 8°–10°. Then the final surface cleaning was operated at a lower beam energy of 2.5 keV and 20 μA to remove the upper copper layer induced by sputtering process.

A film stress tester (FST-1000, Supro Instruments) was used to measure residual stress of the coatings, which were performed on 316L stainless steel substrates (elastic modulus E_s of 195 GPa

and poisson's ratio υ_s of 0.29) based on Stoney's equation [29], as shown below:

$$\sigma = \frac{E_s}{6(1-\upsilon_s)}\frac{h_s^2}{h_c}\left(\frac{1}{R_c}-\frac{1}{R_0}\right) \quad (1)$$

where E_s and υ_s denotes the elastic modulus and poisson's ratio of the substrates, h_s and h_c are the thickness of the substrates and coatings. R_0 and R_c refers the curvature radius before and after the coating deposition, respectively. A nanoindenter (NHT^2, CSM) was performed on YT14 cemented carbides substrates to measure the coating hardness and elastic modulus. A scratch tester (RST, CSM) was used to measure the adhesion strength. The scratch tests were performed at a scratching distance of 3 mm under a maximum load of 80 N. A Vickers hardness tester (MVK-H1, Mitutoyo) was employed to evaluate the toughness of the coatings, and a diamond square cone with a apex angle of θ = 136° was used as the sharp Vickers indenter tip. The indentation tests were conducted on the coatings deposited on the substrates of stainless steel and cemented carbide under a indentation load of 4.9 N with a dwell time of 15 s. The indentation morphologies were then characterized by SEM technique, and the depth of impression d could be calculated by the following formula:

$$d = \frac{a}{2}\cdot\cot(\frac{\theta}{2}) \quad (2)$$

where a and θ refers to the indentation side length and apex angle, respectively.

3. Results and discussion

3.1. Chemical composition and deposition rate

According to the designed spliced target and vertical substrate distances in Fig. 1, various chemical compositions of AlTiVN-Cu coatings can be achieved in Fig. 2(a). When the vertical substrate distance increased from 4 to 22 cm, Cu content increased sharply from 2.6 to 46.7 at.%, whereas both V and N contents decreased linearly from 16.7 to 0.6 at.% and 47.1 to 27.8 at.%, respectively. It indicated that a wide composition range of the coatings can be adjusted with a single spliced target simply by varying the vertical substrate distance. However, due to the special design of $Al_{67}Ti_{33}$-V-Cu spliced target in Fig. 1, all the deposited AlTiVN-Cu coatings contain Cu, and no reference AlTiVN (undoped) coating could be achieved in this study. As shown in Fig. 2(b), the calculated Al/Ti atomic ratios increased gradually from 1.7 to 2.0, closing to the original contents in $Al_{67}Ti_{33}$ alloy target. With the decrease of V content, the (Al+V)/Ti atomic ratios also decreased sharply from 3.0 to 2.1. Moreover, the N/(Al+Ti+V) atomic ratios were within the small range of 0.8 to 1.1, indicating that N content in all the coatings were nearly to the stoichiometric. Due to the different mass between sputtered elements, the variations in atomic ratios could be caused by the re-sputtering effect, especially for the HIPIMS deposition with high ionization degree and ion bombardment.

Fig. 3 shows the deposition rate of AlTiVN-Cu coatings at different Cu contents. With increasing the Cu content from 2.6 to 46.7 at.%, the deposition rate increased linearly from 3.8 to 13.4 nm/min, which can be attributed to the changes in chemical compositions of AlTiVN-Cu coatings. According to the sputtering yields of metals under normally incident Ar^+ ion bombardment [30], the sputtering yields were found to be independent of gas pressure and ion current density, but increasing with ion energy, and raised differently for different materials. At a argon ion energy of 400 eV, the Cu element has the highest sputtering yield of ~1.6 as compared to the Al (~0.8), Ti (~0.4) and V (~0.5) elements. Thus, the increase of deposition rate can be mainly attributed to a sharp increase of Cu content in the deposited coatings.

3.2. Microstructure and residual stress

Fig. 4 displays the XRD patterns of AlTiVN-Cu coatings at different Cu contents. At a low Cu content of 2.6 at.%, it was found that four diffraction peaks centered at about 37.0°, 43.3°, 62.4°,

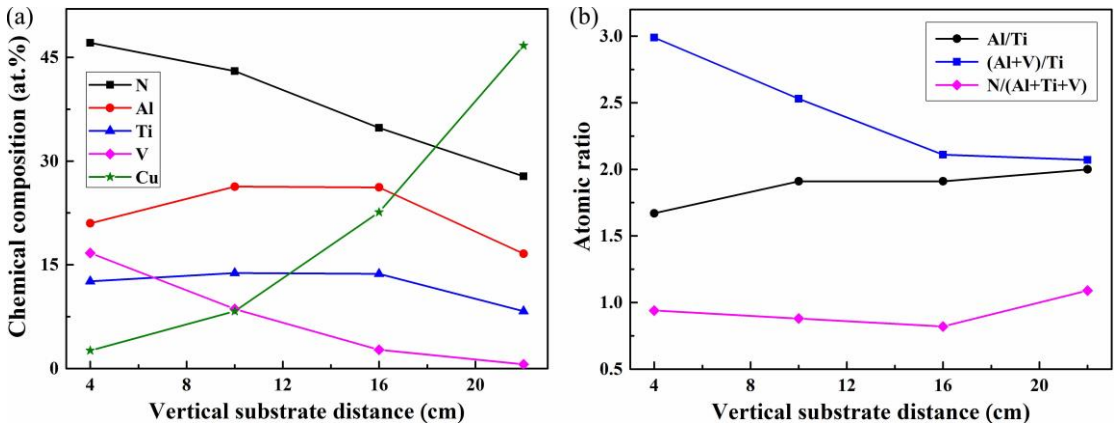

Fig. 2. (a) Chemical composition and (b) atomic ratio of the coatings as a function of vertical substrate distance.

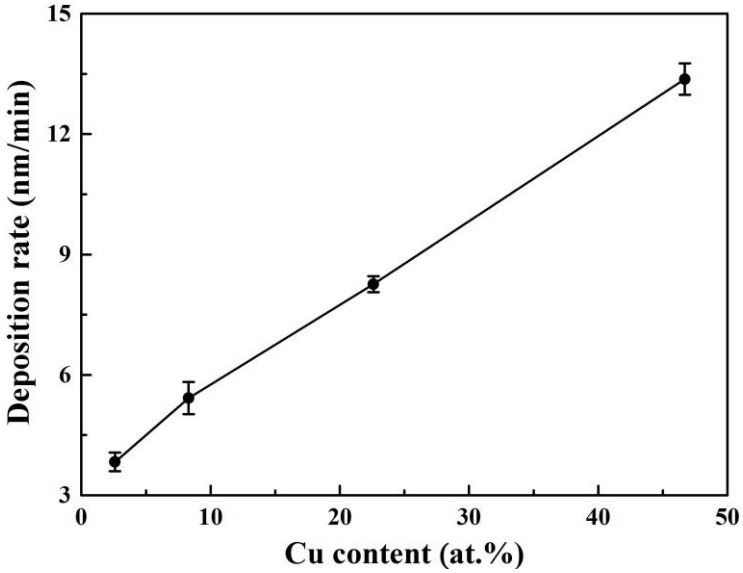

Fig. 3. Deposition rate of AlTiVN-Cu coatings as a function of Cu content.

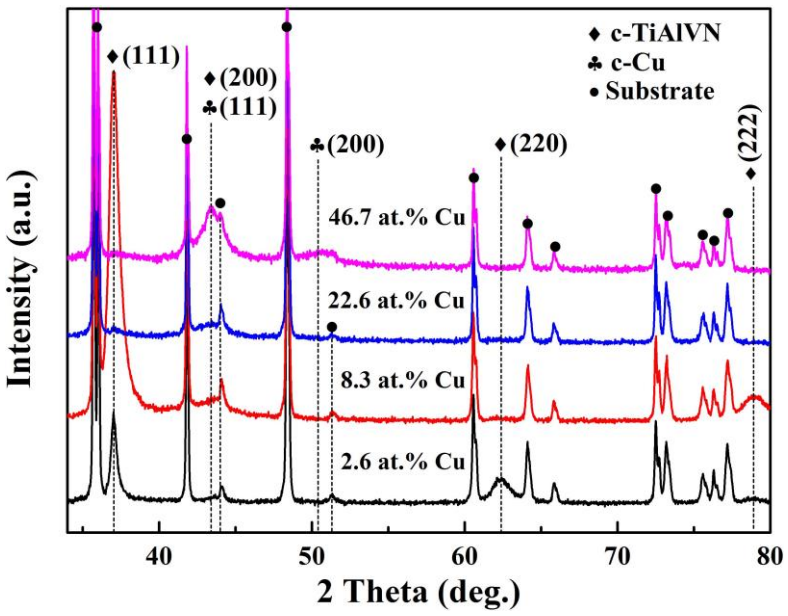

Fig. 4. XRD patterns of AlTiVN-Cu coatings at different Cu contents.

78.9°, which could be corresponded to the (111), (200), (220) and (222) planes of NaCl-type face-centered cubic (FCC) structure, respectively. Due to similar atom radius, the Ti atoms were partly replaced by V and Al atoms in FCC Ti-N lattice, which resulted in the formation of TiAlVN solid-solution phase [19]. It indicated that the V tended to solid solution in FCC TiAlN lattice rather than to form an individual phase of VN in the AlTiVN-Cu coatings. When the Cu content increased up to 8.3 at.%, AlTiVN-Cu coating exhibited an enhanced (111) preferred orientation and the (220)

Table 2 Lattice parameters of AlTiVN-Cu coatings with various Cu contents.

Planes		Lattice parameters a_0 (Å)			
		2.6 at.%	8.3 at.%	22.6 at.%	46.7 at.%
TiAlVN	(111)	4.204	4.203	4.198	—
	(200)	4.178	4.176	4.174	—
	(220)	4.208	—	—	—
	(222)	4.201	4.200	—	—
Cu	(111)	—	—	—	—
	(200)	—	—	—	3.612
Mean		4.198	4.193	4.186	3.612
Stdev		0.013	0.015	0.017	—

peak disappeared. However, when the Cu content further increased to 22.6 at.%, the diffraction peak of (222) disappeared, and the strong preferred orientation of (111) decreased to a extremely low-intensity reflection. Similar results were reported in Zr-Cu-O coatings that the crystallization was strongly suppressed by the incorporation of high Cu content (24 at.%) [26]. When the Cu content reached as high as 46.7 at.%, a new diffraction peak at ~50.5° appeared in the XRD patterns, corresponding to the (200) plane of FCC Cu phase (JCPDS 85-1326). It indicated that the Cu atoms existed as crystalline phase in the AlTiVN-Cu(46.7 at.%) coating. Whereas no obvious nitride phase can be observed in the diffraction peaks, indicating that Cu atoms grew up into metallic crystallites and strongly suppressed the crystal growth of nitride coatings due to repeated nucleation.

In addition, as the Cu content increased, the peak positions shifted slightly toward higher diffraction angles, illustrating that a decrease in lattice parameters. To further quantitatively analyze this variation, the lattice parameters of deposited AlTiVN-Cu coatings were calculated by the Gaussian fittings [31], as listed in Table 2. When Cu content increased from 2.6 to 22.6 at.%, the lattice parameters of AlTiVN-Cu coatings decreased from 4.198 to 4.186 Å. When the Cu content further increased to 46.7 at.%, the lattice parameters decreased sharply to 3.612 Å, which was nearly to the standard reference value (3.615 Å) of Cu powder (JCPDS 85-1326). This further demonstrated that FCC Cu phase formed in AlTiVN-Cu(46.7 at.%) coating. According to the lattice distortion in substitutional solid solutions, the incorporation of Al and V with smaller atomic radius in TiN lattice could lead to lattice shrink as compared to the standard reference value (4.242 Å) of TiN powder (JCPDS 38-1420). Similar results were also found in Ti-Al-V-N coatings that the lattice parameters decreased with the increase of Al and V atoms incorporated in the TiN lattice [19].

Fig. 5 displays the residual stress of AlTiVN-Cu coatings at different Cu contents. All the coatings exhibited a compressive residual stress, which would be caused by the effect of atomic peening during ion bombardment process [32]. When Cu content increased from 2.6 to 46.7 at.%, it can be found that the compressive residual stress decreased sharply from 5.7 to 0.1 GPa, indicating that the compressive residual stress of AlTiVN-Cu coatings can be significantly released by the addition of Cu. Similar results were found in MoN/Cu coatings that the relaxation of residual stress could be mainly attributed to the presence of a compliant copper phase [33].

Fig. 6 shows SEM morphologies of AlTiVN-Cu coating surfaces at different Cu contents. At a low Cu content of 2.6 at.%, AlTiVN-Cu coating exhibited a relatively smooth surface with small microparticles. However, when the Cu content increased to 22.6 at.%, the coating surface became rougher with larger microparticles appeared. Similar results were also reported in TiN-Cu nanocomposite coatings that Cu grains agglomerated around the TiN crystallites, leading to the

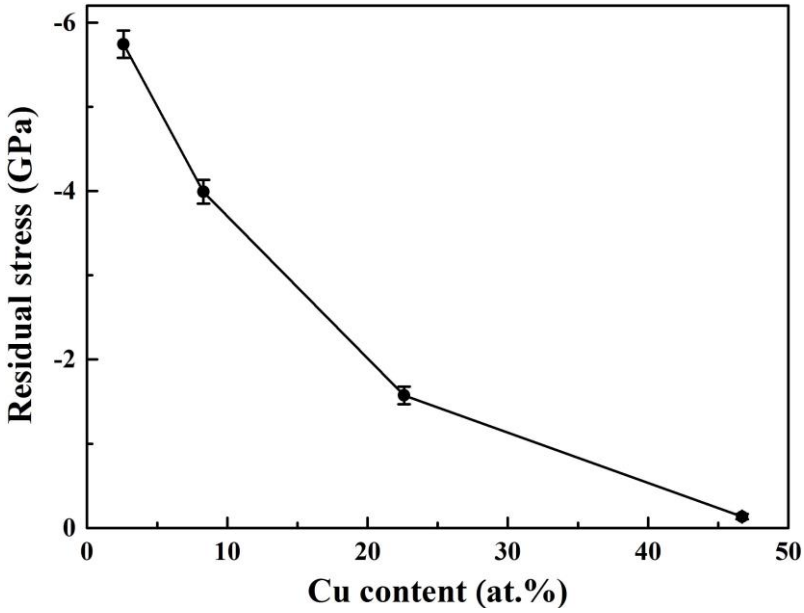

Fig. 5. Residual stress of AlTiVN-Cu coatings as a function of Cu content.

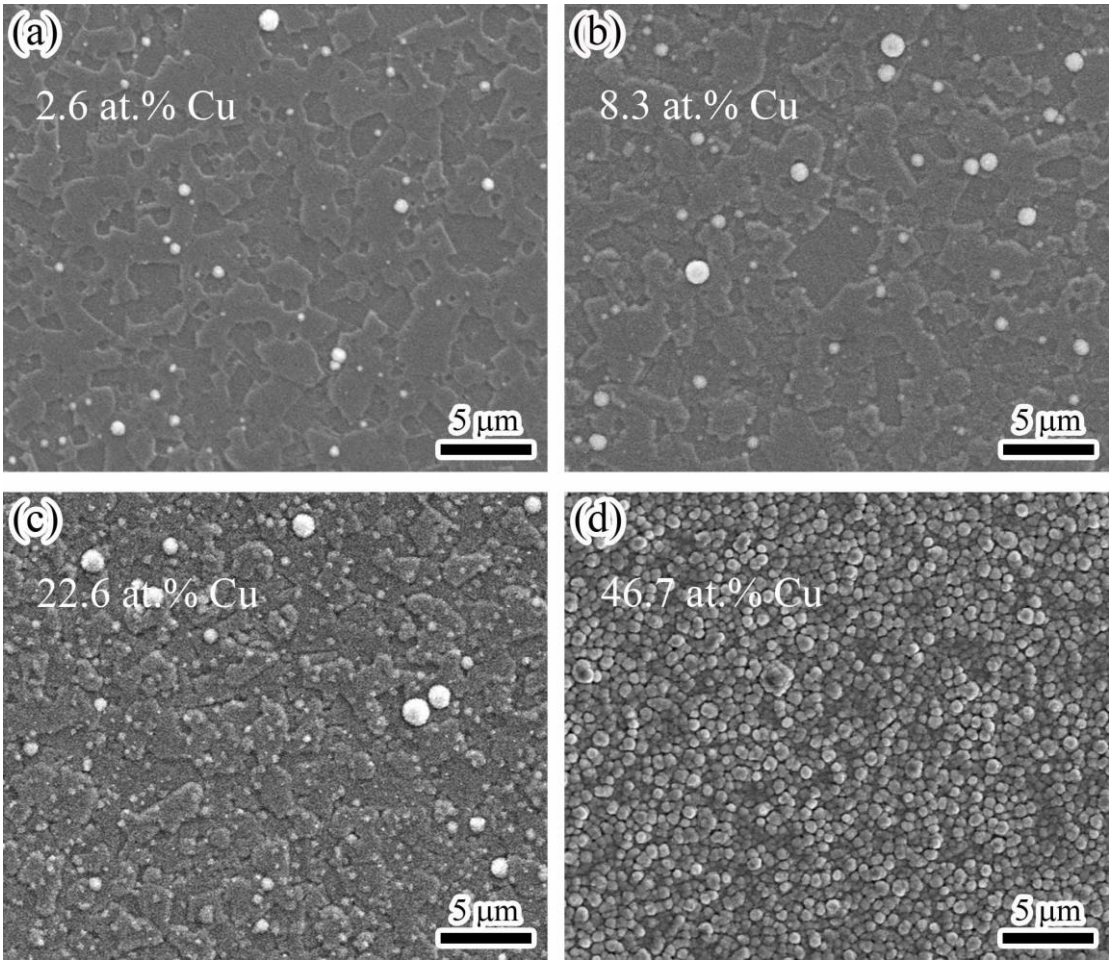

Fig. 6. Surface micrographs of the coatings at different Cu contents: (a) 2.6 at.%, (b) 8.3 at.%, (c) 22.6 at.% and (d) 46.7 at.%.

increase of spherical particles sizes [34]. In Fig. 6(d), when the Cu content reached as high as 46.7 at.%, the coating surface was uniformly covered with many clustered grains, which was typical for a granular structure. At high Cu contents, the atomic mobility increased on the growing surfaces during coating deposition, which led to the immiscible Cu grains clustered to form relatively larger grains [35]. To investigate the surface morphology evolution, three-dimensional AFM images of AlTiVN-Cu coatings at different Cu contents were compared in Fig. 7. At low Cu contents, a plate-like structure can be clearly observed on the coating surfaces. It would be due to the effect of

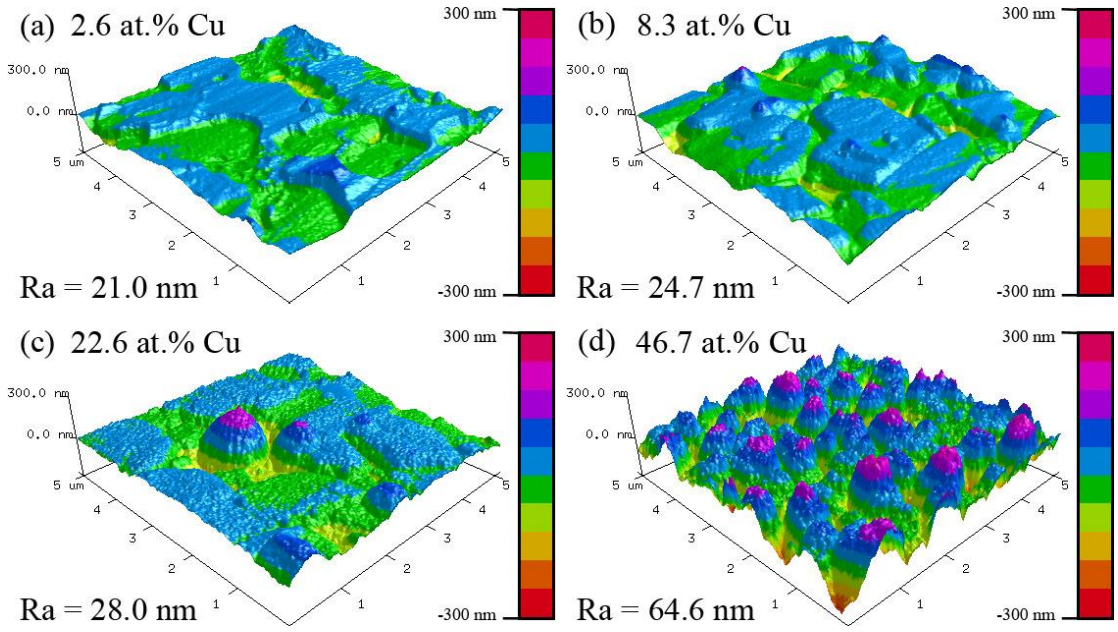

Fig. 7. Three-dimensional AFM images of the coatings at different Cu contents: (a) 2.6 at.%, (b) 8.3 at.%, (c) 22.6 at.% and (d) 46.7 at.%.

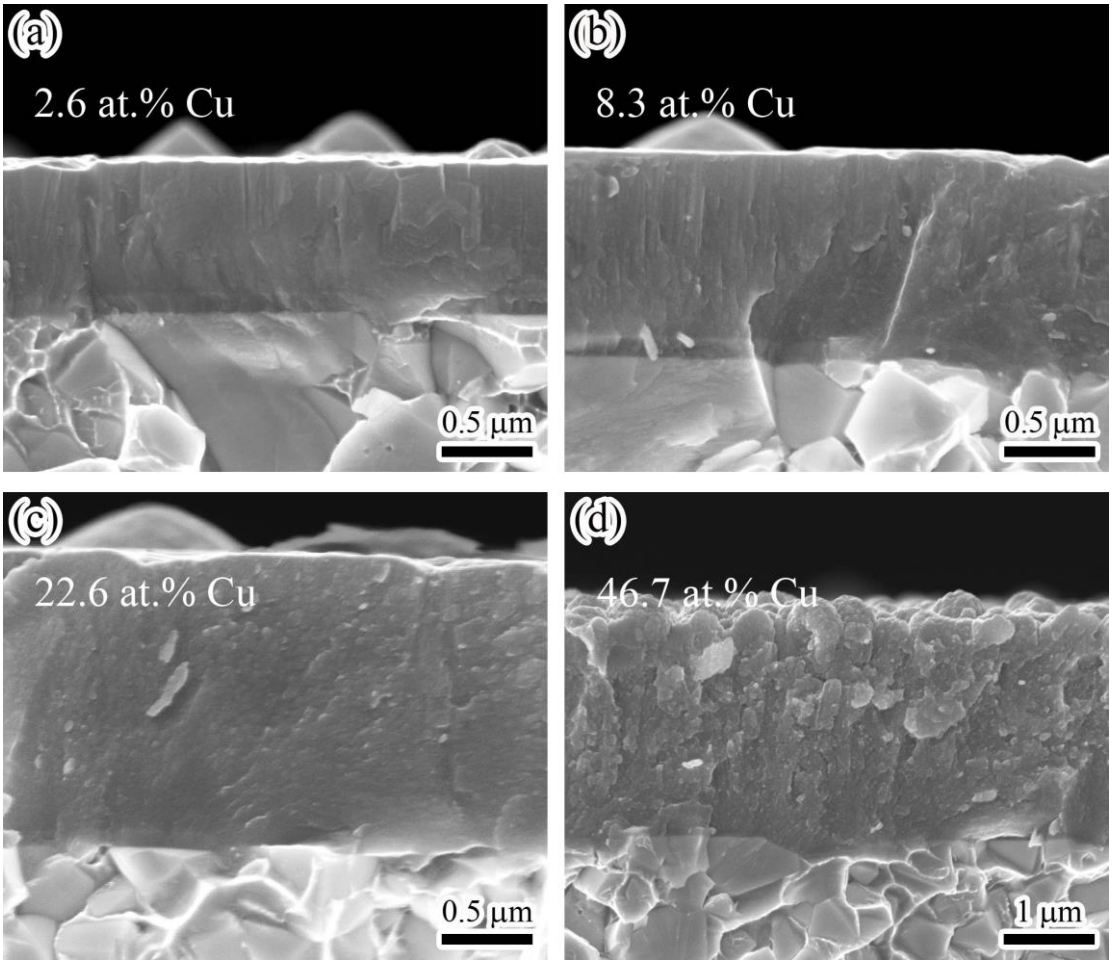

Fig. 8. Cross-sectional SEM micrographs of the coatings at different Cu contents: (a) 2.6 at.%, (b) 8.3 at.%, (c) 22.6 at.% and (d) 46.7 at.%.

strong ion bombardment and etching on the growing coating surfaces, which resulted in a template growth effect of WC-Co substrate. However, when the Cu content increased to 22.6 at.%, the coating surface became rough with small granular structure observed, and then transferred to an island-like structure with larger granular size when the Cu content reached as high as 46.7 at.%,

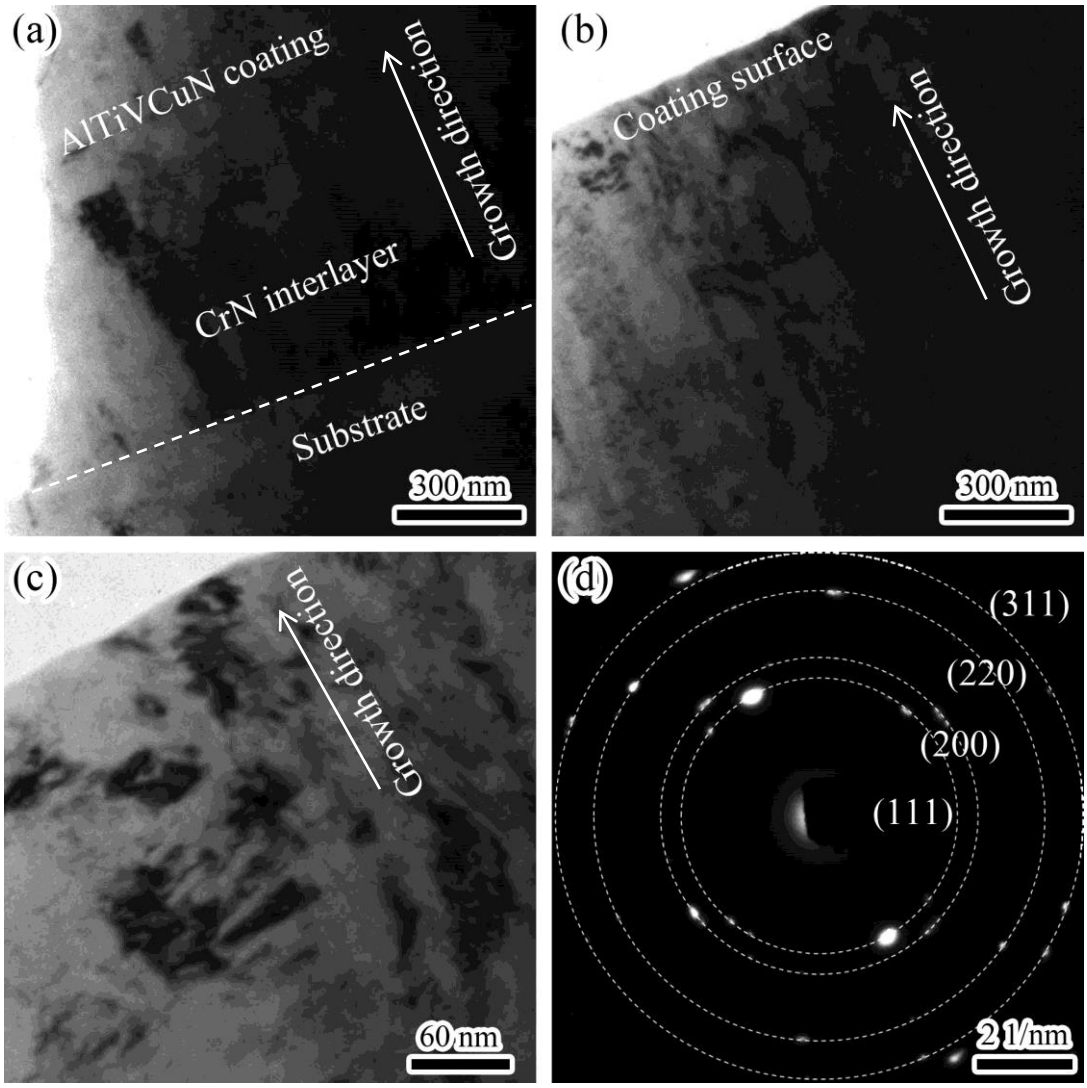

Fig. 9. Cross-sectional TEM bright-field image and selected area electron diffraction pattern of the AlTiVN-Cu(22.6 at.%) coating: (a) lower cross-sectional part, (b) upper cross-sectional part, (c) amplification picture of upper part, (d) SAED pattern.

which could be corresponded to the rough tops of columnar growth. As the Cu content increased, the average surface roughness increased sharply from 21.0 to 64.6 nm, which was in consistent with the surface morphologies observed in Fig. 6.

Fig. 8 displays the fractured cross-sections of AlTiVN-Cu coatings at different Cu contents. As shown in Fig. 8(a, b), AlTiVN-Cu coatings exhibited compact columnar microstructure at low Cu contents, corresponding to II-type structure in Thornton's structure zone model [36]. In addition, a flat and dense interface of YT14 cemented carbide substrate/CrN interlayer/coating can be clearly identified in Fig. 8, indicating that a good adhesion between the substrates and coatings. However, when Cu content increased to 22.6 at.%, a dense fine-grained without obvious columnar microstructure observed in Fig. 8(c), which was in consistent with above XRD results (see Fig. 4). This indicated that the addition of Cu phase into Al-Ti-V-N coatings can significantly influence the microstructure evolution by restricting the growth of columnar crystal, and even formed a dense featureless microstructure. Similar microstructure evolution was also found in Zr-Cu-N nanocomposite coating with a high Cu content of 20 at.% [22]. When Cu content reached as high as 46.7 at.%, AlTiVN-Cu coating exhibited a coarse columnar microstructure. Cu atoms agglomerated in inter-granular boundaries and grew up into metallic Cu crystallites at high Cu contents above 14 at.%, leading to a porous and coarse microstructure in Mo-Cu-N coatings [24].

Fig. 9 displays the bright-field TEM images and selected area electron diffraction (SAED) pattern of AlTiVN-Cu(22.6 at.%) nanocomposite coating. As shown in Fig. 9(a), a bi-layer structure

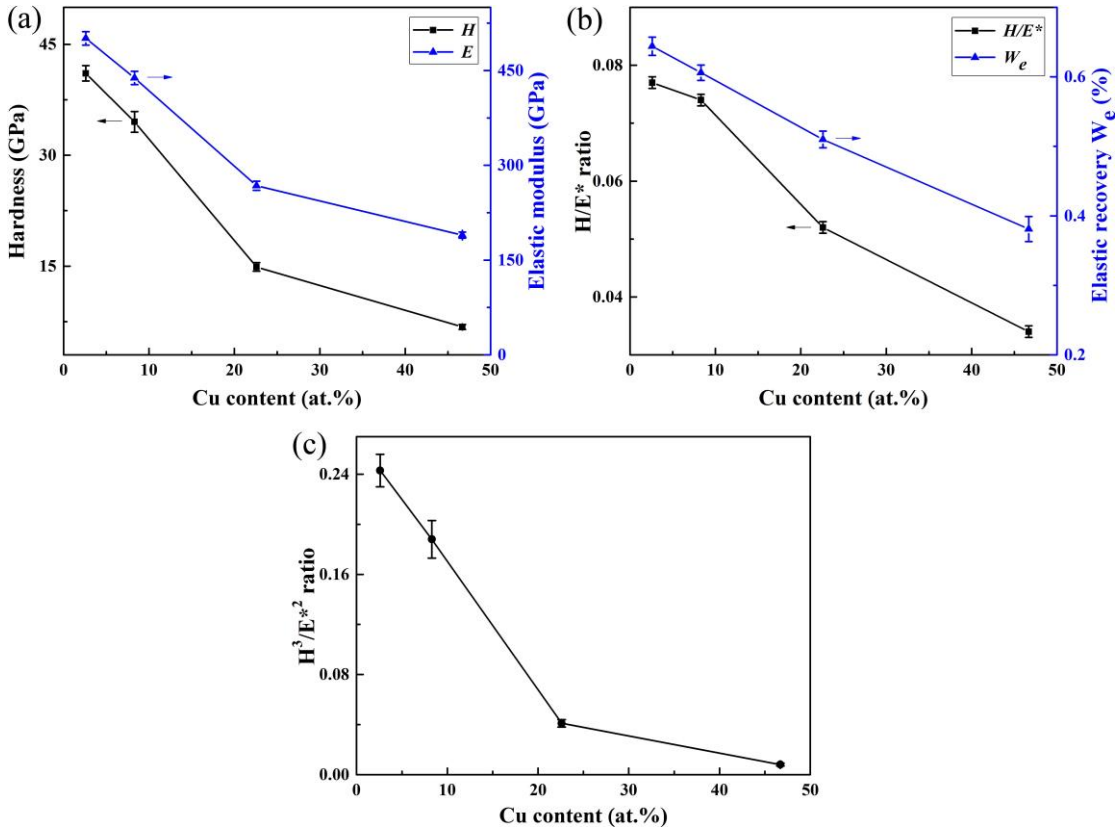

Fig. 10. (a) Hardness *H* and elastic modulus *E*, (b) *H/E** ratio and elastic recovery W_e, and (c) H^3/E^{*2} ratio of the coatings as a function of Cu content.

can be clearly observed, which was in agreement with the cross-section morphology in Fig. 8. The CrN interlayer exhibited a typical columnar structure with a large grain size of 90–110 nm, which was typical for the arc ion plating deposition. As for the upper part in Fig. 9(b), AlTiVN-Cu coating exhibited a extremely fine and incontinuous columnar structure, which was typical for interrupted columnar growth model. It could be explained by Barna and Adamik's structure zone model (SZM) [37], the incorporation of Cu phase in the Al-Ti-V-N coatings blocked the columnar growth and stimulate repeated nucleation, leading to a dense featureless microstructure formed in Fig. 8(c). The corresponding amplification picture of upper part coating as shown in Fig. 9(c), it was found that the short columns with a small grain size of 10–30 nm formed in the upper coating, which demonstrated that the Cu doping contributed to the refinement of crystallite size of TiAlVN phase. In Fig. 9(d), the SAED pattern of upper coating exhibited a typical NaCl-type cubic structure with incontinuous diffraction rings, which can be corresponded to the (111), (200), (220), and (311) planes of TiAlVN solid-solution phase. However, no Cu phase could be identified in the SAED pattern, indicating that Cu atoms existed as an amorphous state in AlTiVN-Cu(22.6 at.%) nanocomposite coating, which was in consistent with above XRD results.

3.3. Mechanical properties

Fig. 10(a) shows the coating hardness and elastic modulus at various Cu contents. At a low Cu content of 2.6 at.%, a relatively high hardness of 41.1 GPa was achieved for the AlTiVN-Cu(2.6 at.%) coating, belonging to the superhard coatings. As for the $Ti_xAl_{2x}V_yN$ coatings, Kutschej et al. reported that the coating hardness increased from 27 to 32 GPa when V content in the target increased from 2 to 10 at.%, which mainly due to the solid solution hardening [17]. The highest hardness of 38 GPa achieved for the coating with 25 at.% V, which caused by the predominantly formed fcc Ti-Al-V-N phase. As for the $Ti_{33-x}Al_{67}V_xN$ coatings, Pfeiler et al. found that increasing V content reduced the fraction of hcp AlN phase in the dual-phase (fcc/hcp) structure, and the highest hardness of 27.5 GPa was obtained for the coating with 16.5 at.% V [18]. As for the $Ti_{16.5}Al_{67}V_{16.5}$ targets, with increasing the bias voltage from -40 to -160 V, the coating hardness increased form 27.6 to 38 GPa, which mainly due to the vanishing of hcp AlN phase and high ion bombardment

Table 3 Nanoindentation test data of AlTiVN-Cu coatings.

Cu content	H (GPa)	E (GPa)	H/E^*	H^3/E^{*2}	W_e	Thickness (μm)	Depth (nm)
2.6 at.%	41.1 ± 1.0	501 ± 11	0.077	0.243	64%	0.8	109
8.3 at.%	34.5 ± 1.4	438 ± 11	0.074	0.188	61%	1.1	119
22.6 at.%	14.9 ± 0.6	268 ± 7	0.052	0.041	51%	1.6	173
46.7 at.%	6.8 ± 0.3	190 ± 5	0.034	0.008	38%	2.5	249

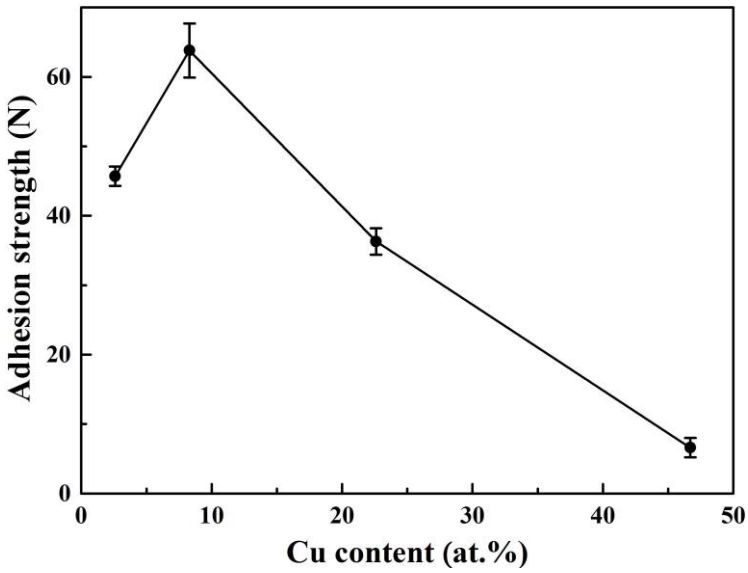

Fig. 11. Adhesion strength of the coatings as a function of Cu content.

induced defect density [38, 39]. Thus, the superhard AlTiVN-Cu(2.6 at.%) coating achieved in this study not only related to the V-alloying but also the addition of Cu.

Due to hardening effect of grain refinement and grain boundary sliding, a small addition of Cu into hard coatings to form nanocomposite structure could also enhance the coating hardness. As for Cr-Cu-N coatings, a high hardness of 35 GPa achieved at a low Cu content of 1 at.% [40]. In Table 3, as Cu content increased to 46.7 at.%, both the coating hardness and elastic modulus sharply decreased to 6.8 GPa and 190 GPa, respectively. The decrease in hardness and elastic modulus would be due to the coarse microstructure and reduced residual stress at high Cu contents. The segregation of Cu into a separate phase, leading to the grains in metallic phase has a tendency to creep under loading [34]. It has been concluded by Musil [41] that a relatively high H/E^* ratio ≥ 0.1 and elastic recovery W_e were expected to achieve the hard nanocomposite coatings with enhanced toughness. In Fig. 10(b), as the Cu content increased from 2.6 to 46.7 at.%, both the H/E^* ratio and elastic recovery W_e decreased linearly from 0.077 to 0.034 and 64% to 38%, respectively. It indicated that the toughness of AlTiVN-Cu coatings reduced when Cu content increased above 2.6 at.%. In Fig. 10(c), the H^3/E^{*2} ratio also decreased sharply from 0.243 to 0.008 when the Cu content increased, implying that the resistance to plastic deformation decreased.

Fig. 11 presents the adhesion strength of AlTiVN-Cu coatings at different Cu contents, which were performed on the cemented carbide substrates. It was reported that the scratch toughness of the coatings could be evaluated by the adhesion strength [42]. When the Cu content increased from 2.6 to 8.3 at.%, the adhesion strength of the coatings increased slightly from 45.7 to 63.8 N, and then followed by a sharp decrease to 6.6 N when Cu content increased to 46.7 at.%. It was found that the improvement in adhesion strength of the hard coatings would be attributed to the combined effects

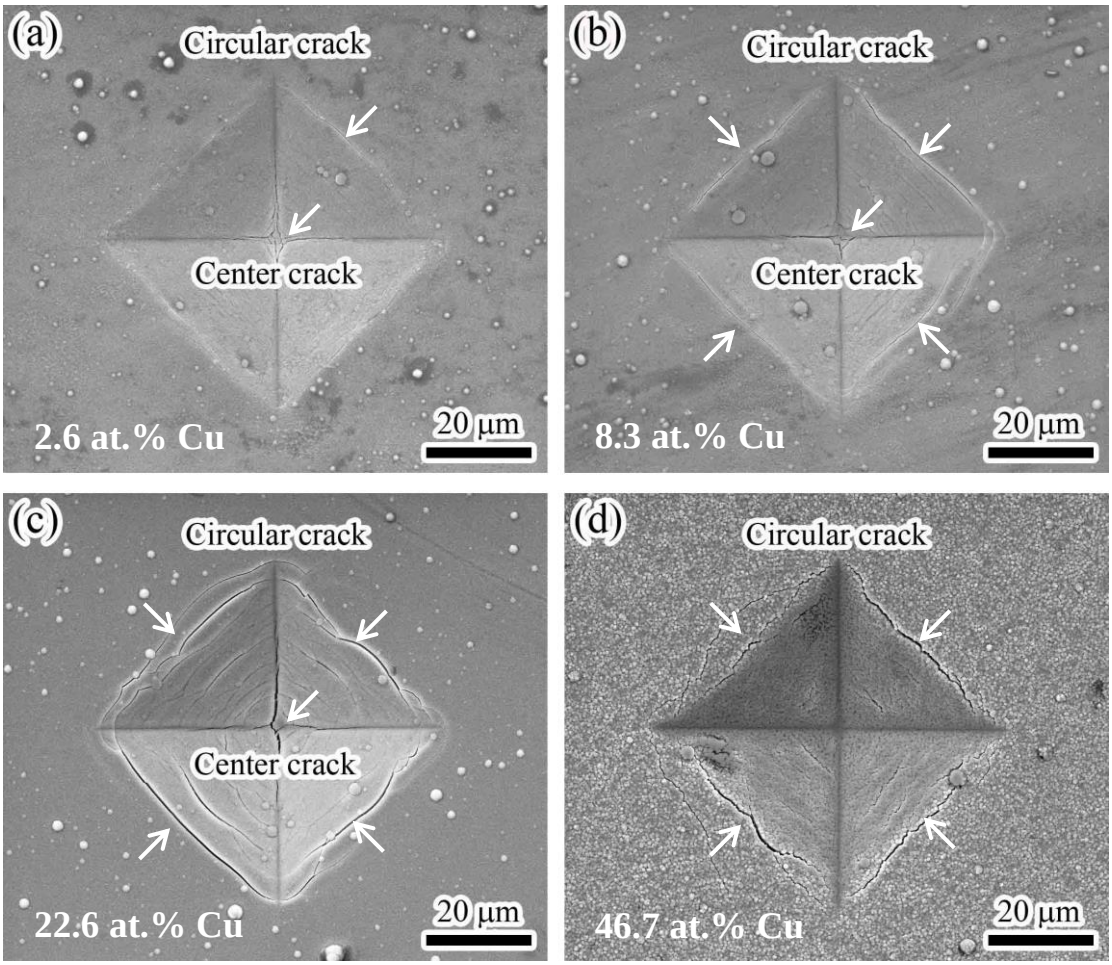

Fig. 12. Vickers indentation SEM images of the coatings performed on 316L stainless steel substrates: (a) 2.6 at.%, (b) 8.3 at.%, (c) 22.6 at.%, (d) 46.7 at.%.

of high H/E^* ratio and appropriate compressive residual stress [43]. Thus, the highest adhesion strength and scratch toughness achieved for AlTiVN-Cu(8.3 at.%) coating would be related to the high H/E^* ratio of 0.074 and appropriate compressive residual stress of 4.0 GPa.

It is well known that the coating toughness refers to the ability to absorb energy during deformation up to fracture, and it can be enhanced and evaluated by the crack resistant. The indentation micrographs of AlTiVN-Cu coatings performed on the 316L stainless steel and YT14 cemented carbides substrates were compared in Fig. 12 and Fig. 13, respectively. As shown in Fig. 12, all the coatings exhibited circular cracks, which was a typical phenomenon of pile up under a high compressive stress [44]. As the Cu content increased, the number of the circular cracks increased, which would be due to the sharp decrease of H^3/E^{*2} ratio in Fig. 10(c). Fig. 13 shows the indentation micrographs of AlTiVN-Cu coatings performed on the cemented carbide substrates. It was found that no obvious cracks observed in Fig. 13(a), implying that AlTiVN-Cu coating exhibited an excellent crack resistant at a relative low Cu content of 2.6 at.%. However, the circular cracks and radial cracks occurred for the AlTiVN-Cu(8.3 at.%) and AlTiVN-Cu(22.6 at.%) coatings, respectively. This phenomenon would be related to the decrease of H^3/E^{*2} ratio and compressive residual stress at high Cu contents. It was reported that high compressive residual stress tended to prevent the formation of radial cracks, while promoted circular cracks [45]. In Fig. 13(d), the coating exhibited no any cracks but plastic deformation when Cu content reached as high as 46.7 at.%. The plastic deformation would be due to the extremely low H^3/E^{*2} ratio of 0.008, and resulted in a low resistance to plastic deformation.

Moreover, center cracks could be clearly identified in the indentation top showed in Fig. 12(a–c). However, no center cracks were found in the coating with a high Cu content of 46.7 at.% in Fig. 12(d). Similar phenomenon were also observed for all the coatings performed on cemented

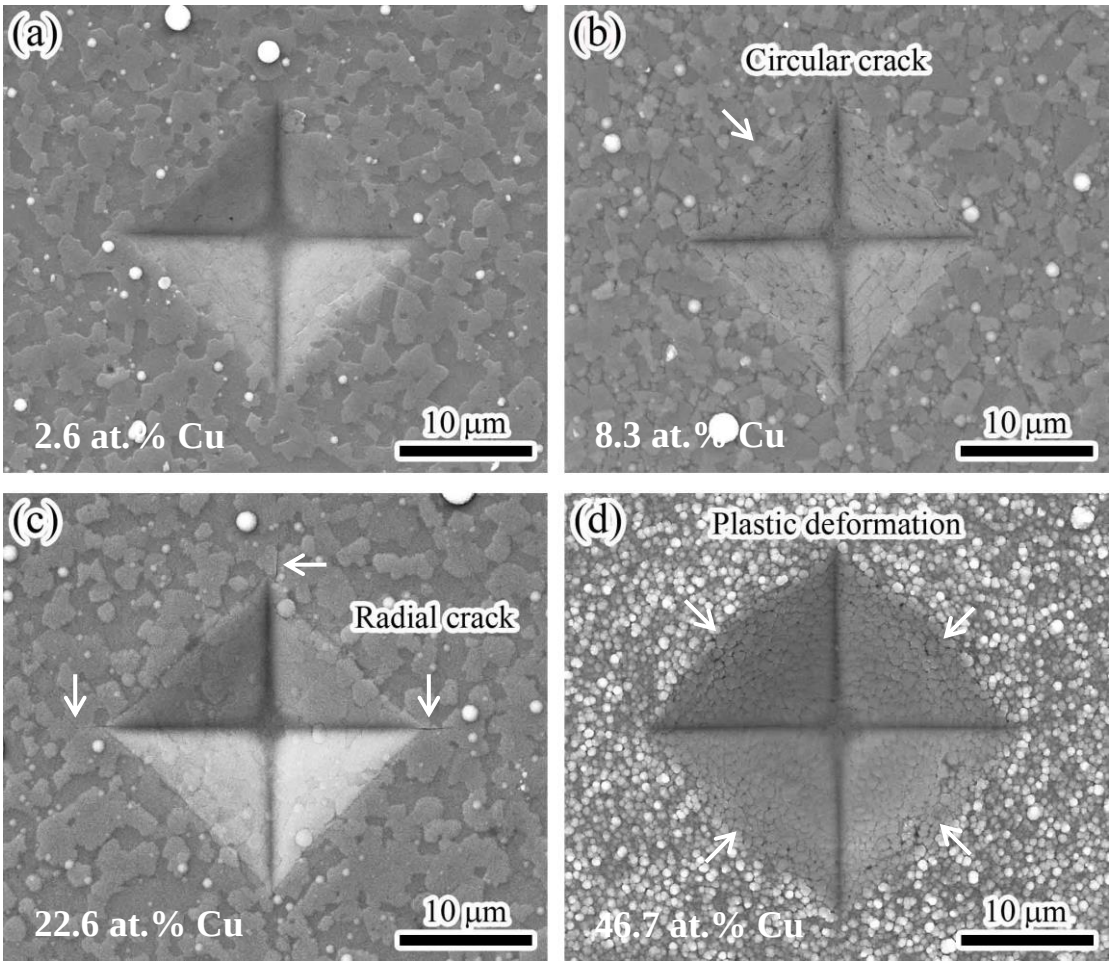

Fig. 13. Vickers indentation SEM images of AlTiVN-Cu coatings performed on YT14 cemented carbide substrates: (a) 2.6 at.%, (b) 8.3 at.%, (c) 22.6 at.%, (d) 46.7 at.%.

carbide substrates in Fig. 13, which would be mainly related to the coating thickness (*h*) and the depth of impression (*d*). As shown in Fig. 14(a), all the depths of impressions were much higher than the coating thickness under a relative high indentation load (L = 4.9 N). In addition, due to the softer substrate of stainless steels, the depth of impressions were much deeper than that of the cemented carbide substrates. In Fig. 14(b), when the Cu content increased, both the *d/h* ratios of stainless steel and cemented carbide substrates decreased from 12.6 to 4.1 and 4.4 to 1.7, respectively. Therefore, to avoid the formation of center cracks, the *d/h* ratio ≤ 4.4 should be ensured as the indentation load increased, especially for the soft substrates.

When compared the indentation images in Fig. 12 and Fig. 13, it demonstrated that the substrates significantly influenced the formation of cracks, which could be related to the mechanical properties of hard coatings (H_c, E_c^*) and substrates (H_s, E_s^*) [46]. As shown in Fig. 14(c−d), when the Cu content increased from 2.6 to 46.7 at.%, both the H_c/H_s ratios of stainless steel and cemented carbide substrates decreased from 9.3 to 1.5 and 2.3 to 0.4, respectively. Similar trends were observed in the E_c^*/E_s^* ratios, which decreased from 2.5 to 0.9 and 0.9 to 0.3 for stainless steel and cemented carbide substrates, respectively. As compared to the hard coatings, the soft substrates suffered much more plastic deformation during loading process, which resulted in a tendency to form circular cracks [26]. Therefore, it can be concluded that AlTiVN-Cu coatings performed on 316L stainless steel substrates with high H_c/H_s ratios ≥ 1.5 and E_c^*/E_s^* ratios ≥ 0.9 would be tended to form the circular cracks. As for the coatings performed on YT14 cemented carbide substrates, no cracks formed in AlTiVN-Cu(2.6 at.%) coating with the highest H^3/E^{*2} ratio of 0.24, and plastic deformation formed in the AlTiVN-Cu(46.7 at.%) coating with an extremely low H^3/E^{*2} ratio of 0.008.

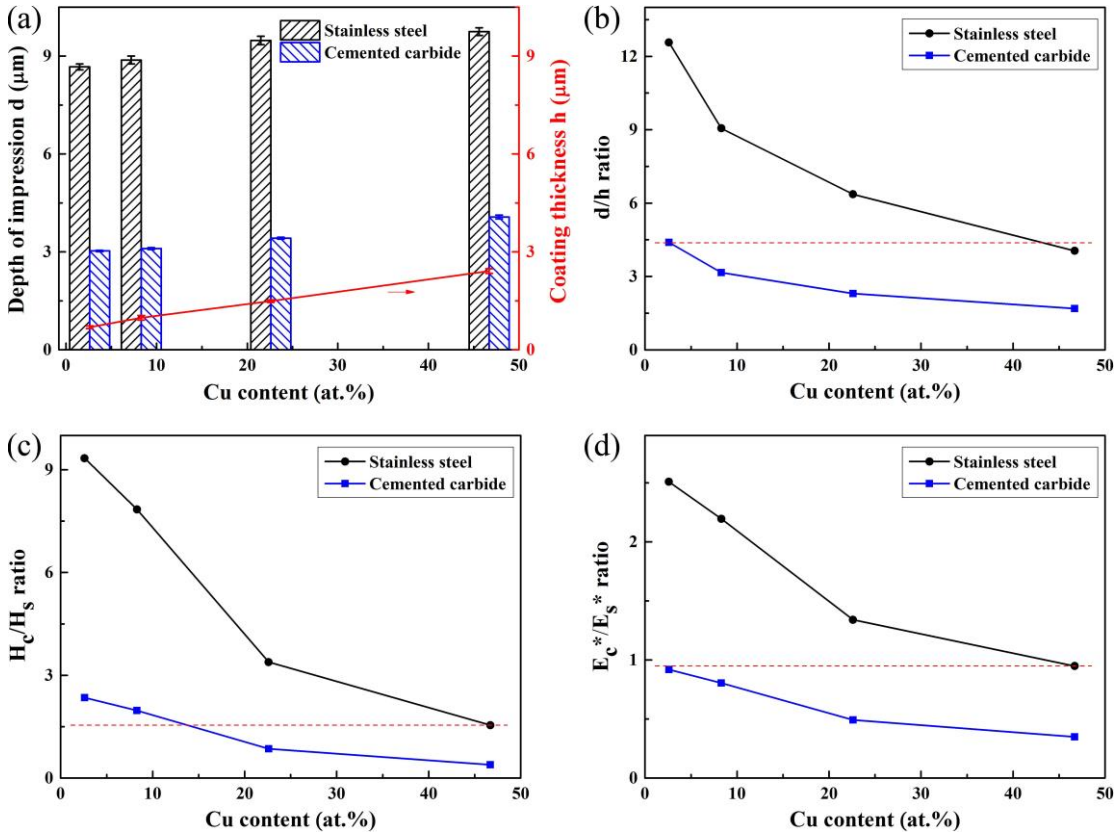

Fig. 14. (a) Depth of impression *d* and coating thickness *h*, (b) *d/h* ratio, (c) H_c/H_s ratio, and (d) E_c^*/E_s^* ratio of the coatings as a function of Cu content.

4. Conclusions

AlTiVN-Cu nanocomposite coatings with various Cu contents were deposited by high power impulse magnetron sputtering with a single $Al_{67}Ti_{33}$-V-Cu spliced target. The various Cu contents in the coatings were simply controlled by altering the vertical substrate positions, and the effect of Cu incorporation on the microstructure evolution and mechanical properties of AlTiVN-Cu nanocomposite coatings was investigated. As the Cu content increased, the microstructure transferred from compact columnar to dense featureless, and then to coarse columnar structure. As the Cu content increased above 22.6 at.%, Cu atoms grew up into metallic crystallites and strongly suppressed the crystal growth of nitride coatings due to repeated nucleation. When the Cu content increased from 2.6 to 46.7 at.%, both the coating hardness and compressive residual stress decreased sharply from 41.1 to 6.8 GPa and 5.7 to 0.1 GPa, respectively. The AlTiVN-Cu(2.6 at.%) coating exhibited an excellent toughness and crack resistant due to the highest H^3/E^{*2} ratio of 0.24. No cracks but plastic deformation formed in AlTiVN-Cu(46.7 at.%) coating due to a extremely low H^3/E^{*2} ratio of 0.008. To avoid the formation of center cracks, *d/h* ratio ≤ 4.4 should be ensured as the indentation load increased, especially for the soft substrates.

Acknowledgements

This work has been initiated by the National Natural Science Foundation of China (Grant No. 51875109), Natural Science Foundation of Guangdong Province (Grant No. 2017A030310665), Middle-aged and Young Teachers' Basic Ability Promotion Project of Guangxi (Grant No. 2018KY0662), Program for Innovative Research Team of Guangdong Province & Huizhou University (IRTHZU), Professorial and Doctoral Scientific Research Foundation of Huizhou University (Grant No. 2020JB010).

References

[1] J. Musil, H. Hrubý, Superhard nanocomposite $Ti_{1-x}Al_xN$ films prepared by magnetron sputtering, Thin Solid Films

365 (2000) 104–109. https://doi.org/ 10.1016/S0040-6090(00)00653-2.

[2] J.D. Bressan, R. Hesse, E.M. Silva, Abrasive wear behavior of high speed steel and hard metal coated with TiAlN and TiCN, Wear 250 (2001) 561–568. https:// doi.org/10.1016/S0043-1648(01)00638-X.

[3] Z.B. Qi, P. Sun, F.P. Zhu, Z.T. Wu, B. Lin, Z.C. Wang, D.L. Peng, C.H. Wu, Relationship between tribological properties and oxidation behavior of $Ti_{0.34}Al_{0.66}N$ coatings at elevated temperature up to 900°C, Surf. Coat. Technol. 231 (2013) 267–272. https://doi.org/10.1016/j.surfcoat.2012.02.017.

[4] S.H. Ahn, J.H. Yoo, Y.S. Choi, J.G. Kim, J.G. Han, Corrosion behavior of PVD–grown WC–$(Ti_{1-x}Al_x)N$ films in a 3.5% NaCl solution, Surf. Coat. Technol. 162 (2003) 212–221. https://doi.org/10.1016/S0257-8972(02)00519-4.

[5] K. Kutschej, P.H. Mayrhofer, M. Kathrein, P. Polcik, C. Mitterer, Influence of oxide phase formation on the tribological behaviour of Ti-Al-V-N coatings, Surf. Coat. Technol. 200 (2005) 1731–1737. https://doi.org/10.1016/j.surfcoat.2005.08. 044.

[6] Y.X. Xu, L. Chen, F. Pei, J.L. Yue, Y. Du, Thermal stability and oxidation resistance of V-alloyed TiAlN coatings, Ceram. Int. 44 (2018) 1705–1710. https: //doi.org/10.1016/j.ceramint.2017.10.100.

[7] Q.S. Ma, L.H. Li, Y. Xu, J.B. Gu, L. Wang, Y. Xu, Effect of bias voltage on TiAlSiN nanocomposite coatings deposited by HiPIMS, Appl. Surf. Sci. 392 (2017) 826–833. https://doi.org/10.1016/j.apsusc.2016.09.028.

[8] F.Y. Gao, G. Li, Y. Xia, Influence of hysteresis effect on properties of reactively sputtered TiAlSiN films, Appl. Surf. Sci. 431 (2018) 160–164. https://doi.org/ 10.1016/j.apsusc.2017.07.283.

[9] Z. Zhou, W.M. Rainforth, Q. Luo, P.E. Hovsepian, J.J. Ojeda, M.E. Romero- Gonzalez, Wear and friction of TiAlN/VN coatings against Al_2O_3 in air at room and elevated temperatures, Acta Mater. 58 (2010) 2912–2925. https://doi.org/ 10.1016/j.actamat.2010.01.020.

[10] Q. Luo, Temperature dependent friction and wear of magnetron sputtered coating TiAlN/VN, Wear 271 (2011) 2058–2066. https://doi.org/10.1016/j.wear.2011.01. 054.

[11] R. Aninat, N. Valle, J-B. Chemin, D. Duday, C. Michotte, M. Penoy, L. Bourgeois, P. Choquet, Addition of Ta and Y in a hard Ti-Al-N PVD coating: Individual and conjugated effect on the oxidation and wear properties, Corros. Sci. 156 (2019) 171–180. https://doi.org/10.1016/j.corsci.2019.04.042.

[12] R. Rachbauer, A. Blutmager, D. Holec, P.H. Mayrhofer, Effect of Hf on structure and age hardening of Ti-Al-N thin films, Surf. Coat. Technol. 206 (2012) 2667– 2672. https://doi.org/10.1016/j.surfcoat.2011.11.020.

[13] A. Magnéli, Structures of the ReO_3-type with recurrent dislocations of atoms: 'homologous series' of molybdenum and tungsten oxides, Acta Cryst. 6 (1953) 495–500. https://doi.org/10.1107/S0365110X53001381.

[14] N. Fateh, G.A. Fontalvo, G. Gassner, C. Mitterer, Influence of high-temperature oxide formation on the tribological behaviour of TiN and VN coatings, Wear 262 (2007) 1152–1158. https://doi.org/10.1016/j.wear.2006.11.006.

[15] R. Franz, C. Mitterer, Vanadium containing self-adaptive low-friction hard coatings for high-temperature applications: A review, Surf. Coat. Technol. 228 (2013) 1–13. https://doi.org/10.1016/j.surfcoat.2013.04.034.

[16] F. Guo, D. Holec, J. Wang, S. Li, Y. Du, Impact of V, Hf and Si on oxidation processes in Ti-Al-N: Insights from ab initio molecular dynamics, Surf. Coat. Technol. 381 (2020) 125125. https://doi.org/10.1016/j.surfcoat. 2019.125125.

[17] K. Kutschej, P.H. Mayrhofer, M. Kathrein, P. Polcik, C. Mitterer, A new low- friction concept for $Ti_{1-x}Al_xN$ based coatings in high-temperature applications, Surf. Coat. Technol. 188–189 (2004) 358–363. https://doi.org/ 10.1016/j.surfcoat. 2004.08.022.

[18] M. Pfeiler, K. Kutschej, M. Penoy, C. Michotte, C. Mitterer, M. Kathrein, The effect of increasing V content on structure, mechanical and tribological properties of arc evaporated Ti-Al-V-N coatings, Int. J. Refract. Met. H. 27 (2009) 502–506. https://doi:10.1016/j.ijrmhm.2008.06.008.

[19] O. Knotek, T. Leyendecker, F. Jungblut, On the properties of physically vapour- deposited Ti-Al-V-N coatings, Thin Solid Films 153 (1987) 83–90. https://doi. org/10.1016/0040-6090(87)90172-6.

[20] O. Knotek, A. Barimani, B. Bosserhoff, F. Löffler, Structure and properties of magnetron-sputtered TiVN coatings, Thin Solid Films 193–194 (1990) 557–564. https://doi.org/10.1016/S0040-6090(05)80065-3.

[21] J. Musil, Hard and superhard nanocomposite coatings, Surf. Coat. Technol. 125 (2000) 322–330. https://doi.org/ 10.1016/S0257-8972(99)00586-1.

[22] P. Zeman, R. Čerstvý, P.H. Mayrhofer, C. Mitterter, J. Musil, Structure and properties of hard and superhard Zr-Cu-N nanocomposite coatings, Mat. Sci. Eng. A289 (2000) 189–197. https://doi.org/10.1016/S0921-5093(00) 00917-5.

[23] J.C. Ding, T.F. Zhang, Z.X. Wan, H.J. Mei, M.C. Kang, Q.M. Wang, K.H. Kim, Influence of Cu content on the

microstructure and mechanical properties of Cr-Cu-N coatings, Scanning 2018 (2018) 1–11. https://doi.org/ 10.1155/2018/6491279.

[24] J.H. Shin, Q.M. Wang, K.H. Kim, Microstructural evolution and tribological behavior of Mo-Cu-N coatings as a function of Cu content, Mater. Chem. Phys. 130 (2011) 870–879. https://doi.org/10.1016/j.matchemphys.2011. 08.002.

[25] H.J. Mei, R. Wang, X. Zhong, W. Dai, Q.M. Wang, Influence of nitrogen partial pressure on microstructure and tribological properties of Mo-Cu-V-N composite coatings with high Cu content, Coatings 8 (2018) 24. https://doi.org/10.3390/ coatings8010024.

[26] M. Jirout, J. Musil, Effect of addition of Cu into ZrO_x film on its properties, Surf. Coat. Technol. 200 (2006) 6792–6800. https://doi.org/10.1016/j.surfcoat.2005.10. 022.

[27] D.S. Belov, I.V. Blinkov, V.S. Sergevnin, N.I. Smirnov, A.O. Volkhonskii, A.V. Bondarev, T.A. Lobova, Abrasive, hydroabrasive, and erosion wear behaviour of nanostructured (Ti,Al)N-Cu and (Ti,Al)N-Ni coatings, Surf. Coat. Technol. 338 (2018) 1–13. https://doi.org/10.1016/j.surfcoat.2018.01.066.

[28] H.J. Mei, Q.S. Luo, X.T. Huang, J.C. Ding, T.F. Zhang, Q.M. Wang, Influence of lubricious oxides formation on the tribological behavior of Mo-V-Cu-N coatings deposited by HIPIMS, Surf. Coat. Technol. 358 (2019) 947–957. https://doi.org/ 10.1016/j.surfcoat.2018.12.033.

[29] G.G. Stoney, The tension of metallic films deposited by electrolysis, Proc. R. Soc. Lond. Ser. A 82 (1909) 172–175. https://doi.org/10.1098/rspa.1909.0021.

[30] N. Laegreid, G.K. Wehner, Sputtering Yields of Metals for Ar^+ and Ne^+ Ions with Energies from 50 to 600 ev, J. Appl. Phys. 32 (1961) 365–369. https://doi.org/ 10.1063/1.1736012.

[31] Q. Luo, Characterization of short-range ordered domains using quantitative X-ray diffraction, Nanosci. Nanotech. Let. 10 (2018) 835–842. https://doi.org/ 10.1166/nnl.2018.2722.

[32] H. Windischmann, Intrinsic stress in sputter-deposited thin-films, Crit. Rev. Solid State 17 (1992) 547–596. https://doi.org/10.1080/10408439208244586.

[33] K.E. Pappacena, D. Singh, O.O. Ajayi, J.L. Routbort, O.L. Erilymaz, N.G. Demas, G. Chen, Residual stresses, interfacial adhesion and tribological properties of MoN/Cu composite coatings, Wear 278–279 (2012) 62–70. https:// doi.org/10.1016/j.wear.2012.01.007.

[34] P. Balashabadi, M.M. Larijani, E. Jafari-Khamse, H. Seyedi, The role of Cu content on the structural properties and hardness of TiN-Cu nanocomposite film, J. Alloy. Compd. 728 (2017) 863–871. https://doi.org/10.1016/j.jallcom. 2017.08. 267.

[35] J.L. He, Y. Setsuhara, I. Shimizu, S. Miyake, Structure refinement and hardness enhancement of titanium nitride films by addition of copper, Surf. Coat. Technol. 137 (2001) 38–42. https://doi.org/10.1016/S0257-8972(00) 01089-6.

[36] J.A. Thornton, High rate thick film growth, Annu. Rev. Mater. Sci. 7 (1977) 239–260. https://doi.org/10.1146/ annurev.ms.07.080177.001323.

[37] P.B. Barna, M. Adamik, Fundamental structure forming phenomena of polycrystalline films and the structure zone models, Thin Solid Films 317 (1998) 27–33. https://doi.org/10.1016/S0040-6090(97)00503-8.

[38] M. Pfeiler, K. Kutschej, M. Penoy, C. Michotte, C. Mitterer, M. Kathrein, The influence of bias voltage on structure and mechanical/tribological properties of arc evaporated Ti-Al-V-N coatings, Surf. Coat. Technol. 202 (2007) 1050–1054. https://doi.org/10.1016/j.surfcoat.2007.07.045.

[39] M. Pfeiler-Deutschmann, P.H. Mayrhofer, K. Chladil, M. Penoy, C. Michotte, M. Kathrein, C. Mitterer, Effect of wavelength modulation of arc evaporated Ti-Al-N/Ti-Al-V-N multilayer coatings on microstructure and mechanical/ tribological properties, Thin Solid Films 581 (2015) 20–24. http://dx.doi.org/10.1016/j.tsf.2014. 10.051.

[40] J. Musil, I. Leipner, M. Kolega, Nanocrystalline and nanocomposite CrCu and CrCu-N films prepared by magnetron sputtering, Surf. Coat. Technol. 115 (1999) 32–37. https://doi.org/10.1016/S0257-8972(99)00065-1.

[41] J. Musil, Hard nanocomposite coatings: thermal stability, oxidation resistance and toughness, Surf. Coat. Technol. 207 (2012) 50–65. https://doi.org/10.1016/ j.surfcoat.2012.05.073.

[42] A.A. Voevodin, J.S. Zabinski, Supertough wear-resistant coatings with 'chameleon' surface adaptation, Thin Solid Films 370 (2000) 223–231. https:// doi.org/10.1016/S0040-6090(00)00917-2.

[43] Y.X. Ou, J. Lin, S. Tong, H.L. Che, W.D. Sproul, M.K. Lei, Wear and corrosion resistance of CrN/TiN superlattice coatings deposited by a combined deep oscillation magnetron sputtering and pulsed dc magnetron sputtering, Appl. Surf. Sci. 351 (2015) 332–343. https://doi.org/10.1016/j.apsusc.2015.05.110.

[44] C.M. Pecnik, D. Courty, D. Muff, R. Spolenak, Fracture toughness of esthetic dental coating systems by nanoindentation and FIB sectional analysis, J. Mech. Behav. Biomed. Mater 47 (2015) 1–11. https://doi.org/ 10.1016/j.jmbbm.2015.03. 006.

[45] Q. Wang, F. Zhou, Z. Zhou, L.K. Li, J. Yan, An investigation on the crack resistance of CrN, CrBN and CrTiBN coatings via nanoindentation, Vacuum 145 (2017) 186–193. https://doi.org/10.1016/j.vacuum.2017.08.041.

[46] J. Musil, M. Jirout, Toughness of hard nanostructured ceramic thin films, Surf. Coat. Technol. 201 (2007) 5148–5152. https://doi.org/10.1016/j.surfcoat.2006.07. 020.